Advanced Functional Materials

Highly Flexible Transparent Electrodes Containing Ultrathin Silver for Efficient Polymer Solar Cells

--Manuscript Draft--

Manuscript Number:	adfm.201503739R1
Full Title:	Highly Flexible Transparent Electrodes Containing Ultrathin Silver for Efficient Polymer Solar Cells
Article Type:	Full Paper
Section/Category:	
Keywords:	transparent electrodes, ultrathin silver, figure-of-merit, flexible polymer solar cells, fill factor
Corresponding Author:	Tonglai Chen ICFO-The Institute of Photonic Sciences Barcelona, SPAIN
Additional Information:	
Question	**Response**
Please submit a plain text version of your cover letter here. **If you are submitting a revision of your manuscript, please do not overwrite your original cover letter. There is an opportunity for you to provide your responses to the reviewers later; please do not add them here**.	Dear Editor, Please find enclosed our manuscript entitled "Highly flexible transparent electrodes containing ultrathin silver for efficient polymer solar cells" by D. S. Ghosh et al., which we would like it is considered for publication in Advanced Functional Materials. There is a growing interest in flexible electronic and optoelectronic devices. These can only be enabled by substrate with transparent conductors which are mechanically flexible. In this work, we introduce a TiO2-Ag-ITO (TAI) transparent electrode (TE) on flexible substrates and demonstrate its use in an inverted polymer solar cell (I-PSCs). The thickness of the top capping ITO layer is only one-third of present state-of-the-art thick ITO (135nm)-TE, thus significantly reducing the consumption of indium, which is scarce and expensive. More specifically the paper contains several breakthroughs: - The TAI-TE exhibits sheet resistance of 6.2 Ohm/sq and optical transmittance of 87.6% between 375-700nm having σ_DC⁄σ_OP ratio close to 500 which is superior to state-of-the-art ITO and other oxide-metal-oxide (OMO) configuration based TEs. - Due to the favourable nucleation and wetting conditions provided by the undercoat TiO2, the ultrathin silver (Ag) film percolates, becomes continuous and shows a high degree of smoothness at very low thicknesses (3-4 nm), much lower than those when it is directly deposited on a plastic or glass substrate. - The developed electrode shows only 6.6% increase in electrical sheet resistance after 1000 tensile bending cycles. These performances, especially in terms of electrical conductivity and mechanical flexibility, are much better than state-of-the-art thick ITO. - Optimized I-PSC, with thinner active layer for enhanced absorption, employing TAI electrodes achieve 8.34% photon conversion efficiency with fill factor (FF) approaching 76% which is among the best in PSCs and comparable with values obtained in inorganic solar cells - The I-PSC fabricated on flexible glass retained 96% of its efficiency after 400 bending cycles. We believe that the results are novel and of great interest for the community of functional materials, in particular in the area of alternative flexible substrates for optoelectronic devices. The results presented holds great potential for large impact on flexible and efficient organic optoelectronic devices. Thank you for considering this manuscript. Sincerely,
Corresponding Author Secondary Information:	
Corresponding Author's Institution:	ICFO-The Institute of Photonic Sciences
Corresponding Author's Secondary	

Institution:	
First Author:	dhriti Sundar Ghosh
First Author Secondary Information:	
Order of Authors:	dhriti Sundar Ghosh
	quan liu
	paola mantilla perez
	Tonglai Chen
	vahagn Mkhitaryan
	Minghuang huang
	Sean Garner
	jordi martorell
	valerio pruneri
Order of Authors Secondary Information:	
Abstract:	Transparent electrodes (TEs) having electro-optical trade-offs better than state-of-the-art indium tin oxide (ITO) are continuously sought as they are essential to enable flexible electronic and optoelectronic devices. In this work, we introduce a TiO2-Ag-ITO (TAI) based TE and demonstrate its use in an inverted polymer solar cell (I-PSCs). Thanks to the favourable nucleation and wetting conditions provided by the TiO2, the ultrathin silver (Ag) film percolates, becomes continuous with high smoothness at very low thicknesses (3-4 nm), much lower than those required when it is directly deposited on a plastic or glass substrate. Compared to conventional ITO-TE, the proposed TAI-TE exhibits exceptionally lower electrical sheet resistance (6.2 Ohm/sq), higher optical transmittance and mechanical flexibility, the latter confirmed by the fact that the resistance increases only 6.6% after 1000 tensile bending cycles. The I-PSCs incorporating the TAI-TE show record power conversion efficiency (8.34%), maintained at 96% even after 400 bending cycles.Also, the TAI-TE exhibits Figure-of-Merit with values close to 500 while ITO reaches 250.

WILEY-VCH

DOI: 10.1002/ ((please add manuscript number))
Article type: Full Paper

Highly Flexible Transparent Electrodes Containing Ultrathin Silver for Efficient Polymer Solar Cells

Dhriti Sundar Ghosh, Quan Liu*, Paola Mantilla-Perez, Tong Lai Chen*, Vahagn Mkhitaryan, Minghuang Huang, Sean Garner, Jordi Martorell, Valerio Pruneri*

Dr. Dhriti Sundar Ghosh, Quan Liu, Paola Mantilla-Perez, Dr. Tong Lai Chen, Vahagn Mkhitaryan, Prof. Jordi Martorell, Prof. Valerio Pruneri
ICFO-Institut de Ciencies Fotoniques, The Barcelona Institute of Science and Technology, 08860 Castelldefels (Barcelona), Spain
E-mail: dhriti.ghosh@icfo.es, quan.liu@icfo.es, tonglai.chen@icfo.es

Dr. Minghuang Huang, Dr. Sean Garner
Corning Incorporated, Sullivan Park, Corning, New York 14831, United States

Prof. Jordi Martorell
Departament de Física i Enginyeria Nuclear, Universitat Politècnica de Catalunya, Terrassa, Spain

Prof. Valerio Pruneri
ICREA- Institució Catalana de Recerca i Estudis Avançats, 08010, Barcelona, Spain

Keywords: transparent electrodes, ultrathin silver, figure-of-merit, flexible polymer solar cells, fill factor

Transparent electrodes (TEs) having electro-optical trade-offs better than state-of-the-art indium tin oxide (ITO) are continuously sought as they are essential to enable flexible electronic and optoelectronic devices. In this work, we introduce a TiO_2-Ag-ITO (TAI) based TE and demonstrate its use in an inverted polymer solar cell (I-PSCs). Thanks to the favourable nucleation and wetting conditions provided by the TiO_2, the ultrathin silver (Ag) film percolates and becomes continuous with high smoothness at very low thicknesses (3-4 nm), much lower than those required when it is directly deposited on a plastic or glass substrate. Compared to conventional ITO-TE, the proposed TAI-TE exhibits exceptionally lower electrical sheet resistance (6.2 Ohm/sq), higher optical transmittance and mechanical flexibility, the latter confirmed by the fact that the resistance increases only 6.6% after 10^3 tensile bending cycles.

The I-PSCs incorporating the TAI-TE show record power conversion efficiency (8.34%), maintained at 96% even after 400 bending cycles. Also, the TAI-TE exhibits Figure-of-Merit with values close to 500 while ITO reaches 250.

1. Introduction

Thin films of Ag have been extensively employed in a variety of applications including plasmonics, optical metamaterials and low-emissivity coatings.[1-3] Another important application of Ag films, in their ultrathin form (thickness <10nm), is transparent electrodes (TEs), which are essential materials in many optoelectronic and photonic devices. For example, in solar cells the TE's transparency permits the light to reach the active layers while their conductivity to collect the generated electrical charges.[4-5] Due to its highest conductivity among metals (1.62×10^{-8} Ω m) and low optical loss in the visible spectrum (refractive index ~0.1), Ag is an ideal material for TEs. In order to improve further the optical transmission of Ag films one can suppress the residual reflections by applying proper undercoat and overcoat layers, typically made of transparent oxides, and achieving in this way oxide-metal-oxide (OMO) structures. The OMO multilayer structure has also the advantage to protect the Ag film from oxidation in the operating environment and from chemical reactions that might arise when in contact with other device layers.[6-7] The electro-optical performances of OMO-TEs are highly related to the inverse relationship existing between electrical conductance and optical transmission. With the metal thickness increasing, the electrical conductance increases while the optical transmission decreases.[8-9]. In addition to increased absorption, a too thick Ag layer would result in strong reflection of visible light, which cannot be efficiently suppressed by the OMO dielectric layers.

It is known that Ag films deposited by physical vapour deposition techniques tend to grow with island-like mode (Volmer-Weber growth mode), consequently exhibit a rough surface morphology with large grain size and high electrical resistivity, which severely affect the

performance of devices.[10-12] Typically, the optimum thickness for ultrathin metals, including Ag films, lies near their percolation, which is defined as the thickness corresponding to which metal islands start to colligate and form a continuous film, resulting in macroscopic electrical conduction.[13-14] Nucleation and wettability are crucial to reduce percolation thickness and increase continuity of the films. Significant research has been carried out to use high energy seed layers,[15-17] self-assembled monolayers (SAMs),[18-19] controlled substrate temperature,[20] co-sputtering Al[21] or oxygen doping[22] to facilitate the uniform and continuous growth of Ag films.

Another crucial aspect of OMO-TEs is the choice of the top oxide layer that, besides the appropriate refractive index and thickness to provide antireflection properties, has to be compatible and possibly enhance the functionality of other layers forming the device, e.g. the electron transport layer in an inverted polymer solar cell (I-PSC).[23-24] So far, in most of the work carried out on OMO-TEs, the top capping layer is a dielectric oxide of 30-50nm thickness characterized by high electrical resistivity.[25-26] In fact, such a thickness is too large for efficient charge extraction/collection in a PSC and this often results in lower fill factor (*FF*) and decreased performance in the PSCs.[27]. A top oxide which is conductive would be extremely beneficial for reducing extraction barrier and collection loss of the separated charges.

Here, we report a TE made of ultrathin Ag film (8nm) in between thin TiO_2 and ITO layers (that we name TAI-TE) which shows very low optical loss (average visible transmittance of ~88%) and extremely low sheet resistance (R_S) (6.2 Ohm/sq). The high refractive index TiO_2 undercoat (bottom) layer facilitates the growth of smooth, highly conductive and continuous Ag film by sputtering method. The Ag thin film is then capped by a thin ITO layer which ensures both electrical conduction and, together with TiO_2 layer, antireflection effect, permitting a high optical transmittance in the visible spectrum. The thickness of the top capping ITO layer is one-third of present state-of-the-art single layer ITO (135nm) electrode, thus also contributing in reducing the consumption of indium, which is scarce and expensive. PSCs

which have shorter energy payback time compared to other photovoltaic technologies were fabricated with the developed TEs.[28] I-PSCs fabricated using TAI-TE show very high performance with photon conversion efficiency (PCE) of 8.34% and enhanced FF (75.7%) for a bulk heterojunction active layer (PTB7:$PC_{71}BM$). The proposed approach can also be applied to plastic substrates, resulting in highly efficient flexible PSCs with superior mechanical properties.

2. Results and Discussion

2.1. Design of TAI electrodes

Ag thin films are highly prone to oxidation and corrosion, even when exposed to ambient atmosphere. For example they can quickly react with small traces of hydrogen sulphide (H_2S) and oxidize, with detrimental effects on their electrical conductivity and transparency.[29] It has been shown that the chemical stability of Ag thin film greatly improves by embedding them in suitable protective layers, as it is the case of stable ITO in the proposed TAI electrode. To design the TAI electrodes i.e., to determine the optimum thicknesses of TiO_2 and ITO layers, Transfer Matrix Method (TMM) was utilized.[30-31] The TMM is a mathematical formalism which is based on Fresnel equations that can be efficiently applied to estimate the optical response of the system including the overall transmittance, reflection of the structure and absorption in each layer. This formalism requires knowledge of the complex refractive index ($\tilde{n}(\lambda) = n(\lambda) + i\kappa(\lambda)$) of the materials. The imaginary part κ (extinction coefficient) is responsible for absorption while the real part n defines the speed of light in the layer. In an ideal case, to maximize the transmittance, besides having low-absorption (κ~0) for both dielectric layers, the bottom layer should have a high n while the capping layer a low n.[25, 32]

In the literature, transmittance of a TE can be given at a specific wavelength, λ=550nm, or as an average value, $T_{ave} = \int_{\lambda_1}^{\lambda_2} T_\lambda d\lambda / \int_{\lambda_1}^{\lambda_2} d\lambda$, over a defined $\lambda_2 - \lambda_1$ range.[33-34] To

accurately compare transmittance for solar applications, in this work we use the average visible transmittance (375-700nm), $T_{ave,solar}$, weighted over the AM1.5G solar spectrum:

$$T_{ave,solar} = \frac{\int_{\lambda_1}^{\lambda_2} I_{AM1.5G}(\lambda)T(\lambda)d\lambda}{\int_{\lambda_1}^{\lambda_2} I_{AM1.5G}(\lambda)d\lambda} \quad (1)$$

Figure 1(a) shows the structure of the TAI-TEs. The $T_{ave,solar}$ was calculated for varying thickness of the bottom TiO_2 and ITO capping layers, between 0 and 100nm, and a constant Ag thin film thickness of 8nm. It can be seen in figure 1 (b) that the effective reflection is strongly dependent on the thicknesses of the TiO_2 and ITO layers and that maximum transmittance can be achieved for ~30nm and ~45nm, respectively. The final optimized TAI-TE geometry was TiO_2(30nm)/Ag(8nm)/ITO(45nm). The optimum thicknesses of dielectric layers do not change significantly for different Ag thin film thicknesses (Figure S1, Supporting Information).

Figure 1(c) shows the wavelength dependent transmission of the TAI-TE corresponding to optimum thicknesses of dielectric layers. For comparison, the transmission of the glass (SiO_2) substrate only, commercial ITO (~135nm thick) on glass, only Ag 8nm thin film on glass and on TiO_2 layer on glass are also shown. Note that for an ITO only TE, the lower the ITO thickness the larger the transparency and the resistance. The transmittance of the TAI electrode is very close to that of the glass substrate. The transmittance of only Ag thin film is comparatively low and is accompanied by a peak in the UV region which corresponds to its characteristic plasma frequency. At longer wavelengths, similar to other metals, its reflection increases. Adding a TiO_2 undercoat layer helps improving the transmittance of Ag thanks to antireflection effect, but the result is still far from the desired performance and that of ITO. Instead, with the ITO top layer the resulting TAI shows transmittance comparable, if not better, to state-of-the-art ITO film. In fact, with TAI configuration and thickness optimization we were able to suppress reflection to values even lower than the blank glass (Figure S2), thus enhancing the

transmittance. For example, the average transmittance between 375-700nm is 87.7% and 85.3% for TAI and ITO, respectively. The large visible transmission of the TE is very advantageous for PSCs, strongly absorbing in this range. The photograph in the inset of Figure 1(c) also confirms the high transparency of the TAI-TE.

2.2. Electrical, Surface and Mechanical Properties of TAI

We measured the electrical resistivity for varying thickness of Ag film on fused SiO_2 substrate with and without the undercoat TiO_2 layer (Figure 1(d)). One can conclude that the TiO_2 layer promoted nucleation and percolation of the Ag films which show low resistivity even at thickness of 4 nm and below.[35] Whereas the Ag film on glass shows already a dramatic increases of resistivity at 6nm. Recently, we observed similar phenomena when a thin Cu seed layer was used to promote seeding and percolation.[15] For the TAI electrode to use in the PSC, we chose an Ag film thickness of 8nm which gives R_S of 6.8 Ohm/sq, further reduced to 6.2 Ohm/sq by the contribution of the 45 nm ITO capping layer.

We also investigated the surface morphology of the deposited film by atomic force microscope (AFM) which confirms the electrical measurement's findings. Figures 2(a), (b) and (c) show the AFM height-profile images of Ag 8nm film deposited on fused SiO_2 substrate, on TiO_2 layer, and also of the overall TAI electrode. The Ag film on fused SiO_2 substrate shows discontinuity characterised by island like structure and large surface roughness (root-mean-square (RMS) roughness of 6.5nm). In fact, the island like morphology is even clearer in the phase diagram of the film (Figure S3, supporting information). Instead, the RMS roughness of the Ag film on TiO_2 layer (2.2nm) was three times smaller, which clearly indicates improvement in film continuity and uniformity thanks to the undercoat TiO_2 layer. The top ITO layer further smoothens the film (RMS roughness of 0.9nm).

Another important aspect associated with TEs is their mechanical flexibility i.e. the retention of electrical properties under multiple bending. The bending test was carried out for TAI films deposited on PET substrate and compared with commercially available thicker ITO on PET.

The bending radius varied from 10mm to 3mm (Figure S4) and the electrical R_S was measured as a function of bending cycles. The maximum bending strain (ε_{MAX}) applied was approximately 2.1%, calculated using the equation $\varepsilon_{MAX} = h_S/(2R)$, where h_S is the thickness of the PET substrate (125µm) and R is the minimum bending radius. The results are shown in Figure 3a. Thanks to the ductility of the Ag layer, the TAI-TE showed a high degree of flexibility with a small relative increase in R_S of 3.8% and 6.6% after 100 and 1000 bending cycles, respectively, while that of ITO was 128% and 770% after only 10 and 100 cycles, respectively. Figure 3b shows the scanning electron microscope (SEM) images of the TEs after bending test. On a large scale, the TAI film is free of any ruptures (Figure 3b1). However some cracks can be seen on a shorter scale with continuous film patches between them (Figure 3b2), which explains the slight increase in R_S. More and longer cracks can be seen for the ITO film (Figure 3b3) which are also more pronounced and deeper compared to the TAI-TEs (Figure 3b4). Note also that the SEM images for TAI-TE is taken after 1000 cycles while for ITO it is taken after a much smaller number (100) of bending cycles.

The trade-off between R_S and optical transmittance (T) were also compared to other recently published OMO structures, with the TAI-TE showing superior performance. A simple way to compare is using a Figure-of-Merit (FoM) defined by ratio of DC conductivity and optical conductivity (σ_{DC}/σ_{OP}) which is related to T and R_S: $T = \left(1 + (Z_0/2R_S)(\sigma_{DC}/\sigma_{OP})\right)^{-2}$ where Z_0 is the free-space impedance.[6, 36] High values of σ_{DC}/σ_{OP} indicated high T and low R_S, respectively. TAI-TE exhibits the highest FoM with values close to 500 while ITO reaches 250 (Table S1).

2.3. I-PSC Performance

To demonstrate the application potential of the highly transparent and low resistance TAI-TE, PSC devices were fabricated with the following structure: Eagle XG Glass/TAI /Sol-gel ZnO (SG-ZnO)/PTB7:$PC_{71}BM$/MoO_3/Ag (Fig. 4a). This inverted device structure has been shown

to have improved ambient stability compared to PEDOT: PSS based direct device structure. The active layer is composed of PTB7:$PC_{71}BM$ bulk heterojunction, which is a well investigated photoactive material, with typical PCE above 7%. [37-39]The reference devices were also fabricated employing standard commercial ITO (135nm) TE on glass substrate.

Initially we fabricated TAI and ITO based devices with an active layer thickness of about 90nm, which was indicated in the literature as the optimal thickness for PTB7:$PC_{71}BM$ structure. [37, 40]. The current density−voltage ($J-V$) characteristics of these I-PSCs were measured (Figures 4c) and the parameters-including the short-circuit current density (J_{SC}), open-circuit voltage (V_{OC}), *FF*, and *PCE* are summarized in Table 1. With 90nm active layer, the ITO-devices exhibited an average J_{SC} of 15.07 mA/cm^2, a V_{OC} of 0.74 V, a *FF* of 72.4%, and an overall *PCE* of 8.11%, whereas the TAI-devices exhibited *PCE* of 7.36±0.10%, with an average J_{SC} of 13.4 mA/cm^2, a V_{OC} of 0.74 V and a *FF* of 74.4%. Clearly, the performance was reduced in TAI-devices mainly because of lower photocurrent compared to ITO counterparts, which is in good agreement with external quantum efficiency (*EQE*) measurements, shown in Figure. 4(d). The *EQE* spectra for TAI devices with 90nm-thick active layer are lower in intensity than those for the ITO counterparts within the 400 to 750nm wavelength range. However, it is worth noting that TAI-devices achieved excellent *FF* with value as high as 75.4%, the highest reported value for the PTB7:$PC_{71}BM$ PSCs. The improved *FF* in TAI-devices can be attributed to the extremely low R_S of the electrode, which reduces the series resistance of I-PSCs (3.02 Ω·cm^2) as compared with ITO-devices (5.78 Ω·cm^2). Generally, a I-PSC with more transparent TE would yield higher photocurrent, but due to optical interference effect, larger electrode transparency does not imply that the light harvesting in the active layer will be enhanced. To further clarify the interference effect of the TAI electrode on photocurrent generation in the corresponding device, we applied TMM to adequately compare the J_{SC} in terms of SG-ZnO and active layer thicknesses for both cases, shown in Figure 5. The optical constants for calculation were taken from literature and details of the model used can be found elsewhere.[41] We

observed that the calculated photocurrent in TAI or ITO based I-PSCs is weakly dependent to the thickness of the SG-ZnO for all given active layer's thicknesses and 20nm thick SG-ZnO offers the best device performance, both theoretically and experimentally. The maximum predicted J_{SC} of ca.15 mA/cm^2 can be found in the ITO-based device when the active layer's thickness is approximately 90nm, which is consistent with earlier reports.[42] In contrast to ITO, J_{SC} in the TAI device reaches the local maximum when the active layer thickness is reduced to 70nm while an increase in the active layer thickness from 70nm to 120nm produces a steady decrease in J_{SC}. Following theoretical predictions, a series of TAI based devices with ca.70nm thick active layer were fabricated and showed average J_{SC} of 14.61 mA/cm^2, V_{OC} of 0.75 V, *FF* of 74.6%, and *PCE* of 8.19%, and the best performance was 8.34%, which is even a little better than the best ITO-based device with a *PCE* of 8.15%. This is among the best reported efficiencies using the ITO/SG-ZnO standard configuration without any additional interfacial modifier, such as PFN.[43] and PEI.[44]. It should be noted that the best FF approaches 76%, which is among the best reported in PSCs and comparable with values obtained in inorganic solar cells.

The opposite J_{SC} variation in TAI-based device is also confirmed by the experimental EQE, which shows spectral enhancement from 450nm to 750nm for TAI-device with 70nm active layer compared to the 90nm counterpart. This enhancement can be attributed to absorption improvement by the optical micro-cavity generated between the thin Ag TAI layer and thick Ag electrodes. Because of the enhanced optical electric field, the optical absorption of the thin active layer is increased, this resulting in EQE enhancement and significant J_{SC} improvement in J_{SC}.[45] Therefore, in PSCs incorporating TAI-TE it is crucial to tune the active layer thickness within the micro-cavity to achieve maximum performance.

We also fabricated I-PSCs incorporating the TAI-TE on flexible Corning® Willow® Glass substrates and evaluated their mechanical flexibility. General properties of flexible glass substrate have been reported previously.[46] Previous reports of flexible glass photovoltaic

devices have included CZTS [47-48] and CdTe structures. [49-50] The photovoltaic parameters were measured as a function of bending radius of curvature and number of cycles, as previously reported. [34] Figures 6(a) and (b) show the parameters with respect to the flat geometry for different radii of curvature. Without any bending stress, devices on Willow Glass exhibited similar performance as their non-flexible glass counterparts, with average J_{SC} of 14.34 mA/cm2, V_{OC} of 0.75 V, *FF* of 75.3%, and *PCE* of 7.98%. When the bending radius is decreased from 5.4 to 2.2 cm, all the parameters remain stable, always above 98% of the flat geometry values. Finally, performances in terms of the number of bending cycles were also measured with the same device and the stability evolution is shown in Figure 6(c) and (d). V_{OC} and J_{SC} remain almost unchanged with only slightly decrease of 1%, while a very small reduction in *FF* indicates slight increase in electrical R_S of the TAI electrode under continuous bending. It has to be noted that different bending radii and bending cycles cases, the *FF* is the parameter mostly affected by the bending stress which results in PCE showing a trend similar to *FF*. Overall, even after 400 bending cycles the I-PSC on flexible glass retained 96% of its initial value.

3. Conclusion

We proposed and developed TiO_2/Ag/ITO based transparent electrodes with sheet resistance of 6.2 Ohm/sq and average optical transmittance of 87.6% between 375-700nm. The developed electrode shows only 6.6% increase in resistance after 10^3 tensile bending cycles. These performances, especially in terms of electrical conductance and mechanical flexibility, are much better than state-of-the-art single layer ITO. Crucially to achieve such performance, the bottom TiO_2 layer promotes a continuous and smooth Ag film while the top ITO film forms a conductive capping layer which together with TiO_2 layer creates an antireflection structure. Optimized inverted polymer solar cells, with thin active layer for enhanced absorption, employing such TAI electrodes achieve 8.34% efficiency, higher than similar structures built on conventional ITO substrates. No significant change in solar cell parameters were observed

under repetitive bending cycles, demonstrating the mechanical robustness of the approach also at device level. The work shows that the proposed TAI transparent electrodes can effectively be used for flexible and efficient organic optoelectronic devices.

4. Experimental Section

TAI deposition and characterization: Double side optically polished UV fused silica/Eagle XG glass substrates, 1 mm thick and 1 inch square was used as substrate. For mechanical flexibility measurements of I-PSCs, Willow Glass (0.140mm thick and 2 inch by 3 inch) was used. Before TE deposition, the substrates were cleaned in acetone followed by ethanol in ultrasonic bath, each process lasting 10 minutes. The substrates were then rinsed in abundant DI water and dried with nitrogen gas followed by low power argon plasma cleaning for 10 minutes inside the sputtering machine. The entire TE structure was prepared by magnetron sputtering without breaking the vacuum. The sputtering chamber was initially evacuated to a base pressure of ~10^{-7}-10^{-8} Torr. The target-to-substrate distance was maintained at 30 cm. The substrate holder was rotating during deposition with a speed of 60 rpm. Ag and TiO_2 were deposited in pure Ar atmosphere while ITO (In_2O_3/SnO_2, 90/10 wt %) was deposited in a mixture of Ar/O_2 (flux ratio 20:1), all of them at room temperature. An Ag (99.99%) target was used to deposit the Ag films using a DC power of 100 W and a working pressure of 2 mTorr. The TiO_2 film was deposited in RF power under the same conditions of the Ag film while the ITO film was deposited at DC power of 60 W and the deposition pressure was maintained at 2 mTorr. The deposition rate was 0.1 Å/s, 2.3 Å/s and 0.7 Å/s for TiO_2, Ag and ITO, respectively. The TAI electrodes were afterwards annealed at 300 °C for 10 minutes at ambient condition. The electrical properties of the films were measured using four-point probe method with cascade Microtech 44/7 S 2749 probe system connected to a Keithley 2001 multimeter. Typically, six measurements were performed at different positions on the films and mean values were used to calculate the R_S. A Perkin Elmer lambda 950 spectrometer was used for optical transmission

measurements. Surface morphology was investigated by a digital instrument D3100 Atomic Force Microscope (AFM) and FEI-Scanning Electron Microscopy (SEM). The AFM image analysis was carried out with Nanoscope 7.30 software.

PSC materials and fabrication: The polymer PTB7 and $PC_{71}BM$ (purity > 99%) were purchased from 1-material and American Dye Source, respectively and were used as received. The sol-gel ZnO precursor solutions (0.3 M) were prepared according to the previously reported method [41, 43]: zinc acetate dehydrate (Zn $(CH_3COO)_2 \cdot 2H_2O$, Aldrich, 99.9%, 0.5 g) and ethanolamine ($NH_2CH_2CH_2OH$, Aldrich, 99.5%, 0.14 g) were dissolved in 2-methoxyethanol ($CH_3OCH_2CH_2OH$, Aldrich, 99.8%, 7.5 mL). This solution was vigorously stirred at 60 °C for 2 hours to complete the hydrolysis reaction in air and then stirred at room temperature for at least 12 hours. Solutions of PTB7:$PC_{71}BM$ (1.0:1.5 wt) at a concentration of 10 mg mL^{-1} were prepared in chlorobenzene with the processing additive 1, 8-diiodoctane (97:3% vol). Devices were fabricated by spin-casting ZnO-Precursor on the pre-cleaned ITO (Lumtec, 135nm, 15 Ω/sq) or TAI glass substrates and annealing at 180 °C in air for 10 min to form a 20nm condensed cathode buffer layer. The prepared samples were then transferred into a N_2-filled glove box for spin-casting the active layer with controlled thicknesses, followed by high-vacuum (< 5×10^{-6} mbar) drying for 1 hour. Finally, MoO_3 (5nm) and Ag (120nm) electrodes were sequentially deposited on the active layer through a shadow mask by thermal evaporation (< 5×10^{-6} mbar), which defines the active area of 0.096 cm^2. The deposition rate was 0.5 Å/s and 1 Å/s for MoO_3 and Ag, respectively.

PSC Characterization: *J–V* curves of all devices were measured with a Keithley 2420 source meter and an Abet Sol3A solar simulator (AM1.5G, 100 mW/cm^2). The illumination intensity of the light source (Xenon lamp, 300W, USHIO) was accurately calibrated employing a standard Si photodiode detector certificated by ISE Fraunhofer. Spectrally resolved EQEs were measured using a bench top QEX10 measurement system supplied by PV Measurements Inc. For the mechanical flexibility measurements, the *J-V* curves were obtained *in situ* at different

radius of curvature while measurements were made after the specified bending cycles in flat configuration.

Supporting Information

Supporting Information is available from the Wiley Online Library or from the author.

Acknowledgements

We acknowledge financial support from the Spanish Ministry of Economy and competitiveness and "Fondo Europeo de Desarrollo Regional" through Grant TEC2013-46168-R and IPT-2012-0986-120000. This project has received funding from the European Union's FP7 research and innovation programme under grant agreement No. 604506. T.L.C. acknowledges financial support through a Ramon y Cajal fellowship. Q.L acknowledges Erasmus Mundus doctorate program Europhotonics (Grant No. 159224-1-2009-1-FR-ERA MUNDUS-EMJD)

Received: ((will be filled in by the editorial staff))
Revised: ((will be filled in by the editorial staff))
Published online: ((will be filled in by the editorial staff))

[1] D. R. Smith, W. J. Padilla, D. C. Vier, S. C. Nemat-Nasser, S. Schultz, *Phys. Rev. Lett.* **2000**, 84, 4184.

[2] T. J. Yen, W. J. Padilla, N. Fang, D. C. Vier, D. R. Smith, J. B. Pendry, D. N. Basov, X. Zhang, *Science* **2004**, 303, 1494.

[3] N. Fang, H. Lee, C. Sun, X. Zhang, *Science* **2005**, 308, 534.

[4] D. S. Ghosh, *Ultrathin Metal Transparent Electrodes for the Optoelectronics Industry,* Springer Theses, **2013**.

[5] D. S Hecht, L. Hu, G. Irvin, *Adv. Mater.* **2011**, 23, 1482.

[6] D. S. Ghosh, T. L. Chen, N. Formica, J Hwang, I Bruder, V Pruneri, *Sol. Energy Mater. Sol. Cells* **2012**, 107, 338.

[7] J. Zou, C-H Li, C-Y Chang, H-L. Yip, A. K-Y. Jen, *Adv. Mater.* **2014**, 26, 3618.

[8] T. Winkler, H. Schmidt, H. Flügge, F. Nikolayzik, I. Baumann, S. Schmale, T. Weimann, P. Hinze, H-H. Johannes, T. Rabe, S. Hamwi, T. Riedl, W. Kowalsky, *Org. Elec.* **2011**, 12, 1612.

[9] N. P. Sergeant, A. Hadipour, B. Niesen, D. Cheyna, P. Heremans, P. Peumans, B. P. Rand, *Adv. Mater.* **2012**, 24, 728.

[10] M. Hu, S. Noda, H. Komiyama, *Surf. Sci.* 2002, 513, 530.

[11] D. Gu, C. Zhang, Y-K. Wu, L. J. Guo, *ACS Nano* 2014, 8, 10343.

[12] M. Ohring, Materials Science of Thin Films, 2nd ed.; Academic Press: San Diego, CA, 2002; Vol.1, p 386.

[13] L. Martínez, D.S. Ghosh, S. Giurgola, P. Vergani, V. Pruneri, *Opt. Mater.* **2009**, 31 (8), 1115.

[14] T. L. Chen, D. S. Ghosh, D. Krautz, S. Cheylan, V. Pruneri, *Appl. Phys. Lett.* **2011**, 99 (9), 093302.

[15] N. Formica, D. S Ghosh, A. Carrilero, T. L. Chen, R. E Simpson, V. Pruneri, *ACS Appl. Mater. Inter.* **2013**, 5 (8), 3048.

[16] S. Schubert, J. Meiss, L. M. Meskamp, K. Leo, *Adv. Energy Mater.* 2013, 3, 438.

[17] V. J. Logeeswaran, N. P. Kobayashi, M. S. Islam, W. Wu, P. Chaturvedi, N. Fang, S. Y. Wang, R. S. Williams, *Nano Lett.* **2009**, 9, 178.

[18] H. M. Stec, R. Williams, T. S. Jones, R. A. Hatton, *Adv. Funct. Mater.* **2011**, 21, 1709.

[19] A. Kossoy, V. Merk, D. Simakov, K. Leosson, S. Kéna-Cohen, S. A. Maier, *Adv. Opt.* **2015**, Mater.3, 1.

[20] S. E. Roark, K. L. Rowlen, *Anal. Chem.* 1994, 66 (2), 261.

[21] C. Zhang, D. Zhao, D. Gu, H. Kim, T. Ling, Y-K. R. Wu, L. J. Guo, *Adv. Mater.* **2014**, 26, 5696.

[22] W. Wang, M. Song, T-S. Bae, Y. H. Park, Y-C. Kang, S-G. Lee, S-Y. Kim, D. H. Kim, S. Lee, G. Min, G-H. Lee, J-W. Kang, J. Yun, *Adv. Funct. Mater.* **2014**, 24, 1551.

[23] D. W. Zhao, P. Liu, X. W. Sun, S. T. Tan, L. Ke, A. K. K. Kyaw, *Appl. Phys. Lett.* **2009**, 95, 153304.

[24] D.W. Zhao, S.T. Tan, L. Ke, P. Liu, A.K.K. Kyaw, X.W. Sun, G.Q. Lo, D.L. Kwong, *Sol. Energy Mater. Sol. Cells* **2010**, 94, 985.

[25] D. R. Sahu, J-L. Huang, *Mater. Sci. Eng. B* **2006**, 130, 295.

[26] K. Jeon, H. Youn, S. Kim, S. Shin, M. Yang, *Nanoscale Res. Lett.* **2012**, 7, 253.

[27] J. Krantz, M. Richter, S. Spallek, E. Spiecker, C. J. Brabec, *Adv. Funct. Mater.* **2011**, 21, 4784.

[28] S. B. Darling, F. You, *RSC Adv.* **2013**, 3, 17633.

[29] J. L. Elechiguerra, L. Larios-Lopez, C. Liu, D. Garcia-Gutierrez, A. Camacho-Bragado, M. J. Yacaman, *Chem. Mater.* **2005**, 17 (24), 6042.

[30] J. Chilwell, I. Hodgkinson, *J. Opt. Soc. Am. A* **1984**, 1, 742.

[31] K-S. Chen, H-L Yip, J-F. Salinas, Y-X. Xu, C-C Chueh, A. K-Y. Jen, *Adv. Mater.* **2014**, 26, 3349.

[32] K. Hong, J. H. Son, S. Kim, B. H. Koo, J-l. Lee, *Chem. Commun.* **2012**, 48, 10606.

[33] V. D. Groep, P. Spinelli, A. Polman, *Nano. Lett.* **2012**, 12, 3138.

[34] A. Bou, P. Torchio, S.Vedraine, D. Barakel, B. Lucas, J-C. Bernède, P-Y. Thoulon, M. Ricci, *Sol. Energy Mater. Sol. Cells* **2014**, 125, 310.

[35] N. Formica, P. Mantilla-Perez, D.S. Ghosh, D. Janner, T.L. Chen, M. Huang, S. Garner, J. Martorell, V. Pruneri, *ACS Appl. Mater. Interfaces* **2015**, 7, 4541.

[36] L. Hu, D. S. Hecht, G. Gruner, *Nano Lett.* **2004**, 4, 2513.

[37] A. M. Otero, Q. Liu, P. M. Perez, M. M. Bajo, J. Martorell. *J. Mater. Chem. A* **2015**, 3, 10681.

[38] Y. Y. Liang, Z. Xu, J. B. Xia, S.-T. Tsai, Y. Wu, G. Li, C. Ray, L. Yu, *Adv. Mater.* **2010**, 22, E135.

[39] L. Lu, L. Wu, *Adv. Mater*. **2014**, 26, 4413.

[40] S. Loser, B. Valle, K. A. Luck, C. K. Song, G. Ogien, M. C. Hersam, K. D. Singer, T. J. Marks, *Adv. Energy Mater.* **2014**, 4: 1301938

[41] R. Betancur, A. Martinez-Otero, X. Elias, P. Romero-Gomez, S. Colodrero, H. Miguez, J. Martorell, *Sol. Energy Mater. Sol. Cells.* **2012**, 104, 87.

[42] S. Loser, B. Valle, K. A. Luck, C. K. Song, G. Ogien, M. C. Hersam, K. D. Singer, T. J. Marks, *Adv. Energy Mater.* **2014**, 4, 1301938.

[43] Y.-M. Chang and C.-Y. Leu, *J. Mater. Chem. A* 2013, 1, 6446–6451

[44] S. Woo, W.H. Kim, H. Kim, Y. Yi, H.K. Lyu, Y. Kim. *Adv. Energy Mater.* **2014**, 4, 1301692

[45] W. Yu, L. Shen, F. Meng, Y. Long, S. Ruan, W. Chen. *Sol. Energy Mater. Sol. Cells* **2012**,100, 226.

[46] S. Garner, S. Glaesemann, X. Li, *Appl. Phys. A* **2014**, 116, 403.

[47] C-Y. Peng, T.P. Dhakal, S.M. Garner, P. Cimo, S. Lu, C.R. Westgate, *IEEE T. Device Mat. Re.* **2014**, 14, 121.

[48] C-Y. Peng, T.P. Dhakal, S. Garner, P. Cimo, S. Lu, C.R. Westgate, *Thin Solid Films* **2014**, 562, 574.

[49] W.L. Rance, J.M. Burst, D.M. Meysing, C.A. Wolden, M.O. Reese, T.A. Gessert, W.K. Metzger, S. Garner, P. Cimo, T.M. Barnes, *Appl. Phys. Lett.* **2014**, 104, 143903.

[50] J.M. Burst, W.L. Rance, D.M. Meysing, C.A. Wolden, W.K. Metzger, S.M. Garner, P. Cimo, T.M. Barnes, T.A. Gessert, M.O. Reese, *IEEE-PVSC, Denver*, June **2014**.

Figure 1. (a) Transparent electrode structure studied in this work. (b) Simulated average visible (375-700nm) transmittance of TAI electrode weighted over the AM1.5G solar spectrum for

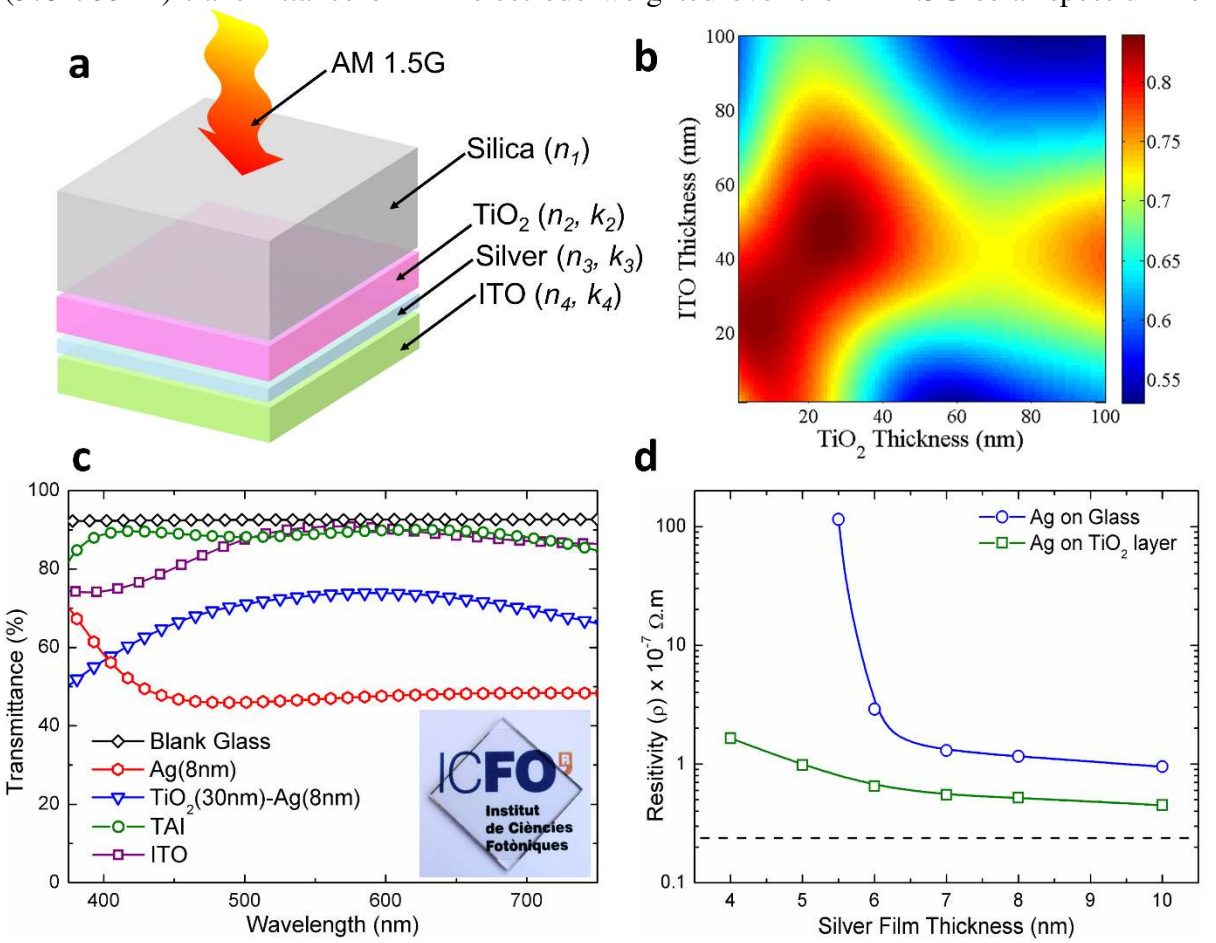

different thicknesses of TiO_2 and ITO for Ag 8nm film. (c) Wavelength dependent optical spectra of TAI electrode compared to other films and the SiO_2 substrate (the transmission values include the substrate contribution). (d) Comparison of electrical resistivity variation for Ag films with and without a bottom TiO_2 seed layer. The dashed line represents the resistivity of bulk Ag film of about 300nm thickness deposited using the same sputtering process.

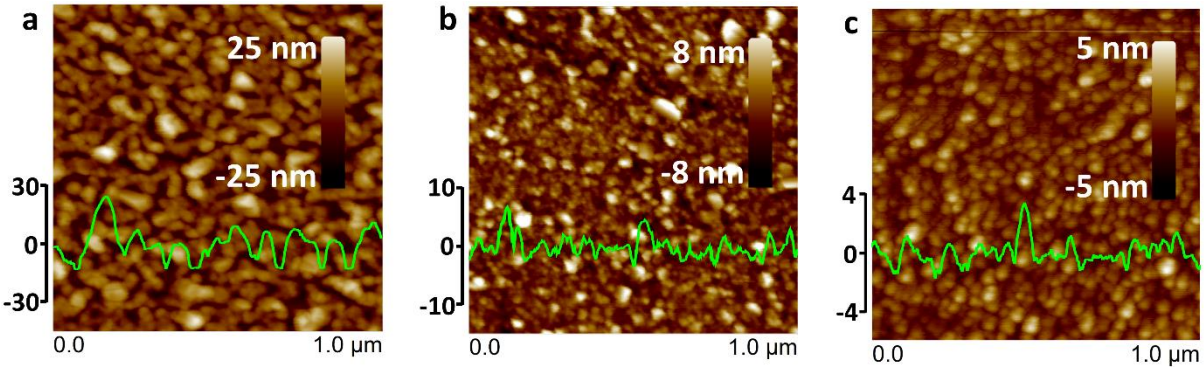

Figure 2. (a) Atomic force microscopy and typical cross section profilometry of (a) Ag 8nm, (b) TiO_2 30nm-Ag 8nm, (c) TAI-TE

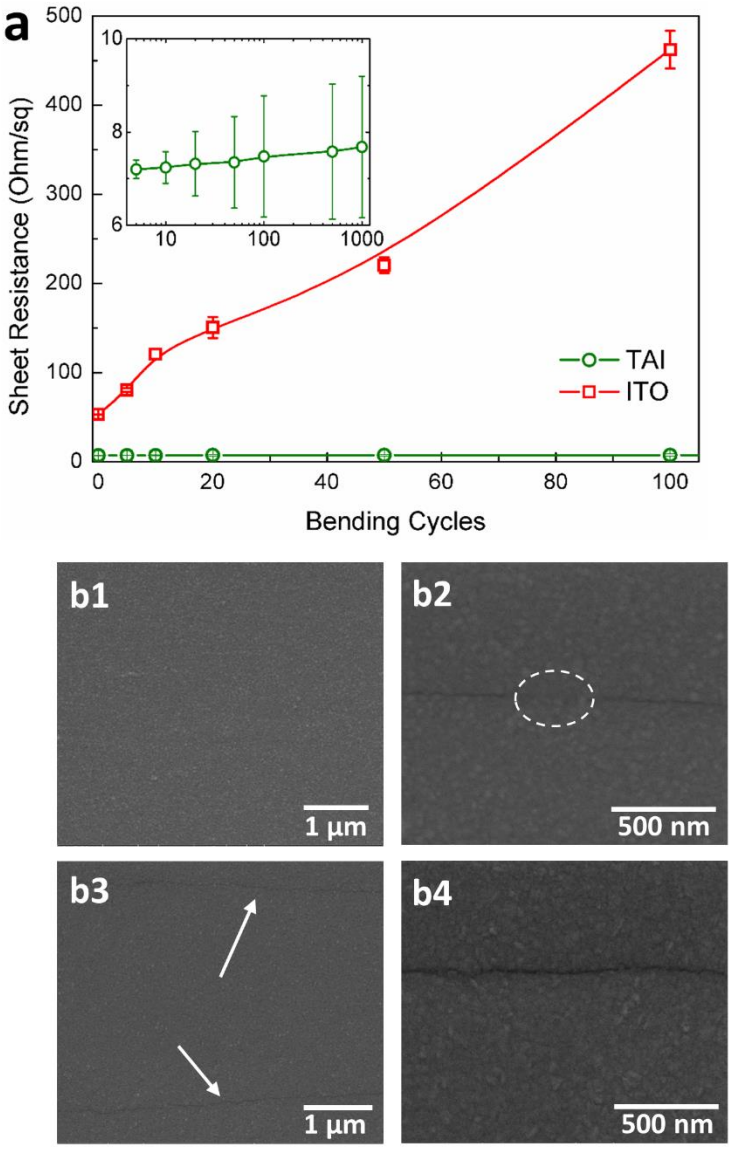

Figure 3. (a) Change in R_S after bending as a function of bending cycles for TAI-TEs and conventional ITO-TEs. Inset shows the same for a larger number of bending cycles for TAI-TE. (b) Scanning electron microscope images of TAI (b1, b2) and ITO (b3, b4) TE films after bending. The dashed oval in (b2) shows an area with continuous film in between a crack while the arrows in (b3) shows two crack lines running parallel to the direction of tensile bending.

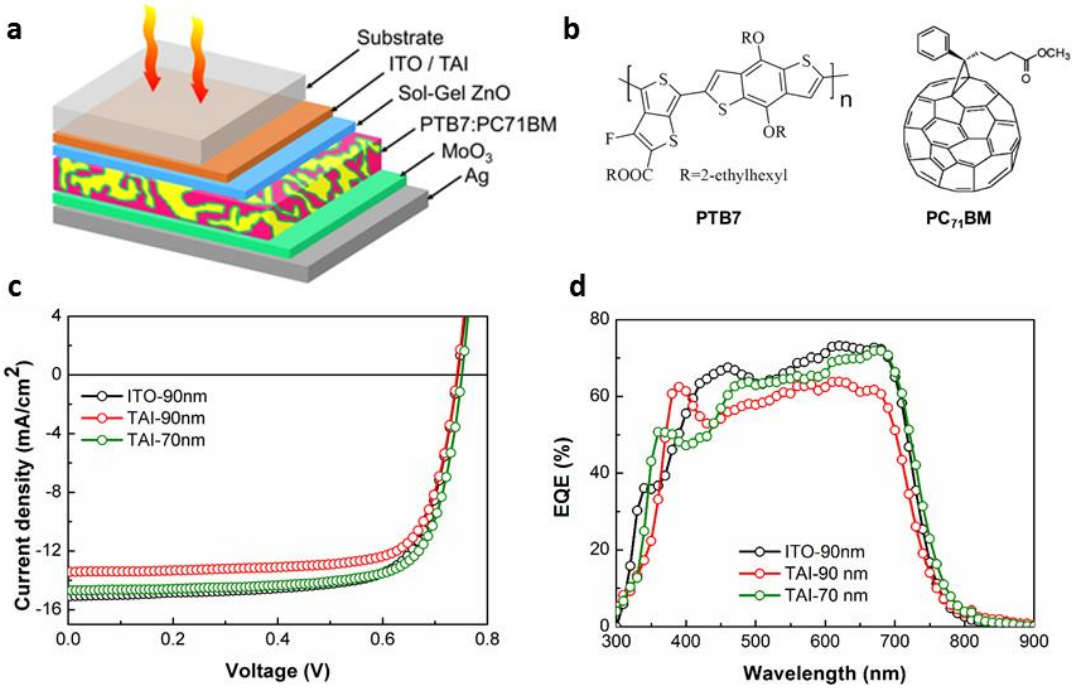

Figure 4. (a) Device architecture of I-PSCs. (b) Molecular structures of PTB7 and $PC_{71}BM$. (c) J-V curves of I-PSC under simulated 100 mW/cm^2 AM1.5G illumination. The values indicate active layer thickness. (d) EQE spectra of best-performing I-PSCs

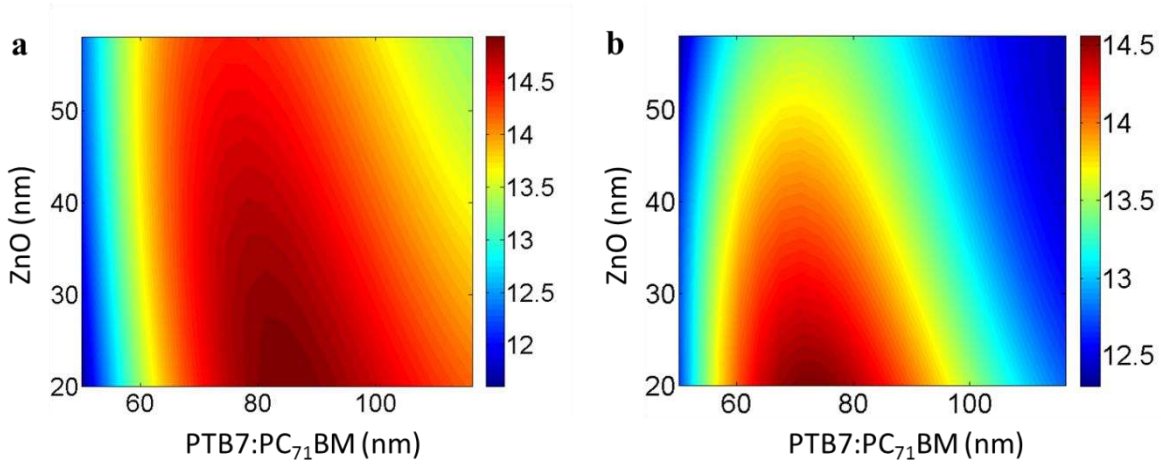

Figure 5. (a) Contour plot of the numerically calculated J_{SC} as a function of the sol-gel ZnO and active layer thickness. (a)ITO-based device. (b) TAI-based device.

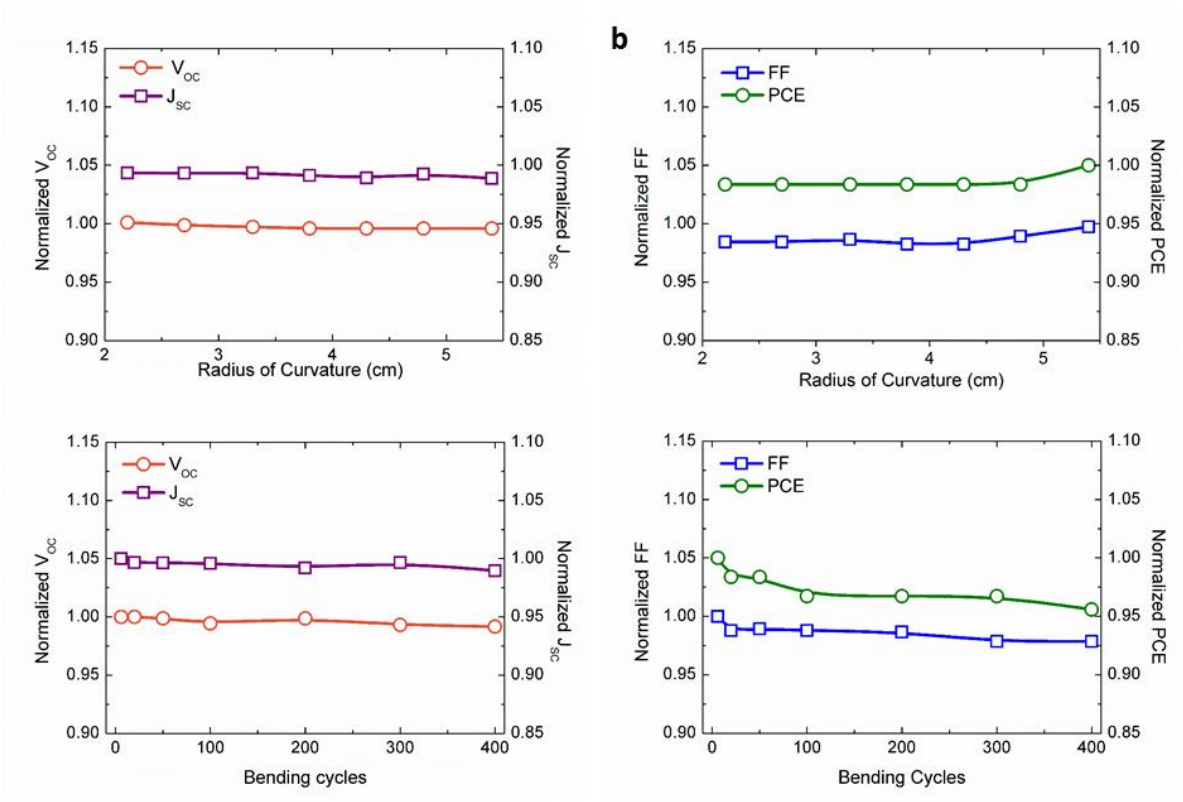

Figure 6. Different solar cell parameters as a function of (a)(b) radius of curvature, (c)(d) bending cycles. For (a), (b) the *J-V* curves were obtained *in situ* at different radius of curvature while for (c), (d) measurements were carried out in flat configuration after bending.

Table 1. Photovoltaic performance comparison of PTB7:$PC_{71}BM$ solar cells on standard ITO/glass and TAI/glass substrates.

Substrate	J_{SC} [mA/cm^2]	V_{OC} [V]	FF [%]	PCE [%]	J_{SC} (EQE) [d] [mA/cm^2]	R_{Series} [Ω·cm^2]
Standard ITO/glass	15.07 (15.07±0.11) [a]	0.74 (0.74)	72.8 (72.4±0.4)	8.15 (8.11±0.04)	15.32	5.78
TAI/glass [b]	13.44 (13.39±0.08)	0.74 (0.74)	75.4 (74.4±0.6)	7.52 (7.36±0.10)	13.42	3.02
TAI/glass [c]	14.66 (14.61±0.09)	0.75 (0.75)	75.7 (74.6±0.6)	8.34 (8.19±0.11)	14.94	2.67
TAI/Corning® Willow® Glass [c]	14.33 (14.35±0.19)	0.75 (0.75)	75.8 (74.9±0.6)	8.06 (7.96±0.13)	14.53	2.97

[a] Average values and standard deviation of device statistics from over 6 devices are given in parentheses; [b] Non-optimized device (active layer thickness=90nm); [c] Optimized device (active layer thickness=70nm). [d] Calculated from the EQE spectra.

We developed TiO2/Ag/ITO based transparent electrodes (TEs) with sheet resistance of 6.2 Ohm/sq and average optical transmittance in the visible of 87.6%, these performances being superior to those of state-of-the-art single-layer ITO. Polymer solar cells employing such TEs achieved 8.34% efficiency, higher than similar structures on conventional ITO substrates. The work shows that the proposed TEs have great potential in flexible optoelectronic devices.

transparent electrodes, ultrathin silver, figure-of-merit, flexible polymer solar cells, fill factor

Dhriti Sundar Ghosh*, Quan Liu, Paola Mantilla-Perez, Tong Lai Chen*, Vahagn Mkhitaryan, Minghuang Huang, Sean Garner, Jordi Martorell, Valerio Pruneri

Highly Flexible Transparent Electrodes Containing Ultrathin Silver for Efficient Polymer Solar Cells

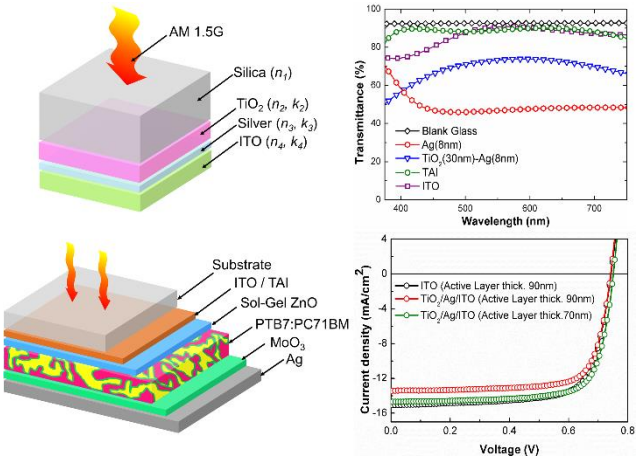

Supporting Information

Highly Flexible Transparent Electrodes Containing Ultrathin Silver for Efficient Polymer Solar Cells

Dhriti Sundar Ghosh, Quan Liu, Paola Mantilla-Perez, Tong Lai Chen*, Vahagn Mkhitaryan, Minghuang Huang, Sean Garner, Jordi Martorell, Valerio Pruneri*

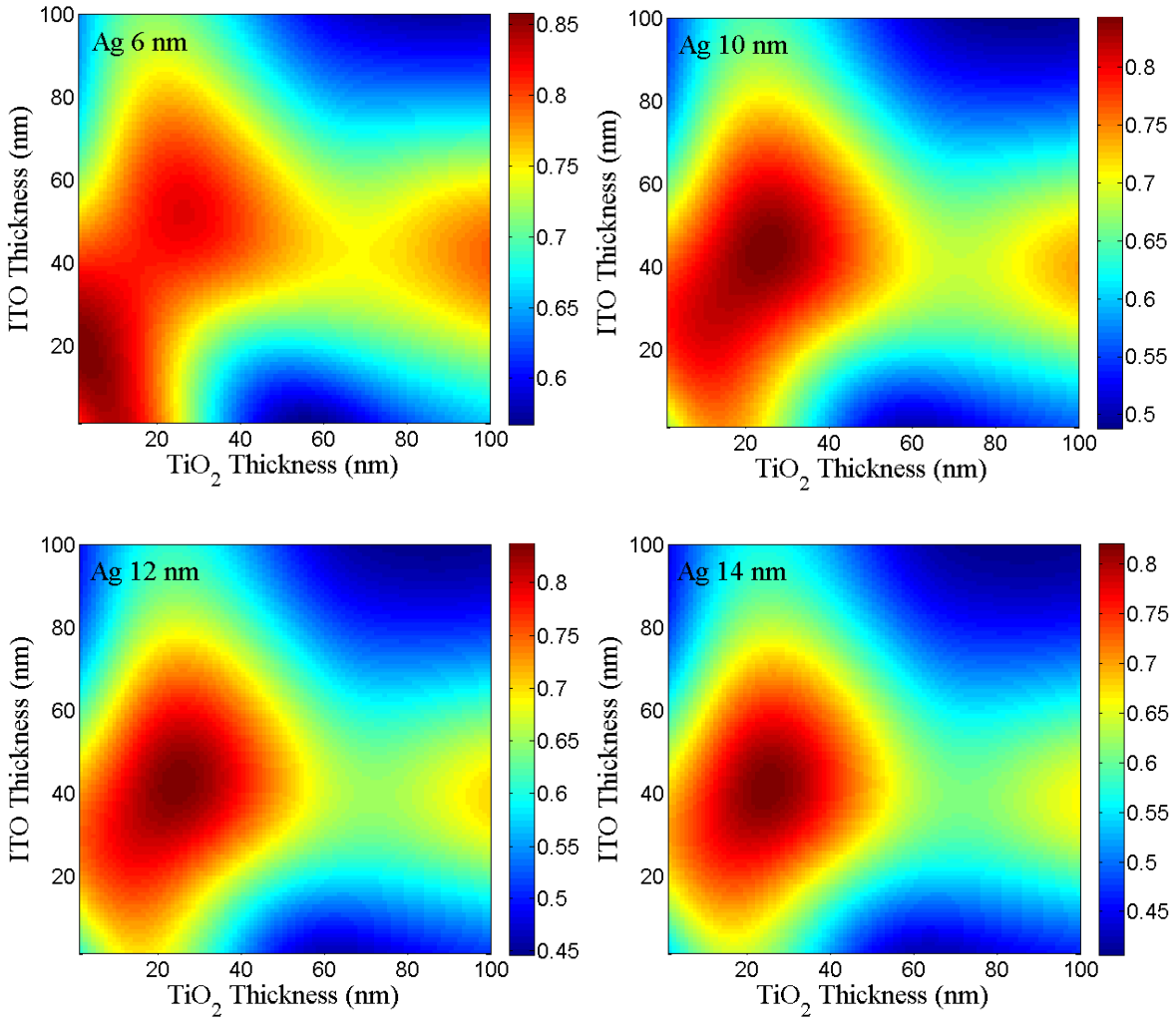

Fig. S1. Simulated mean visible transmittance between 375-700nm for different thicknesses of bottom TiO_2 and top ITO layer for (a) Ag 6nm, (b) 10nm, (c) 12nm, (d) 14nm

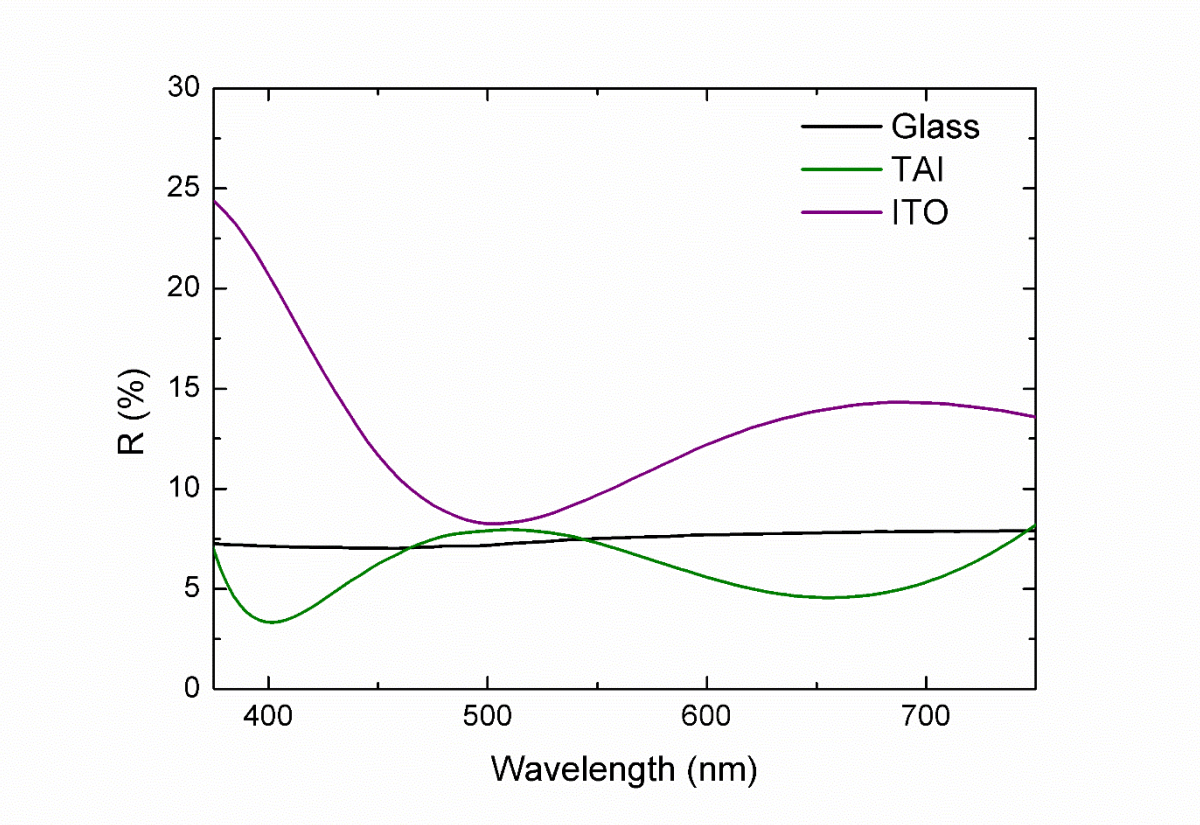

Fig. S2.Reflection measurements of the TAI electrode comparing with glass and ITO.

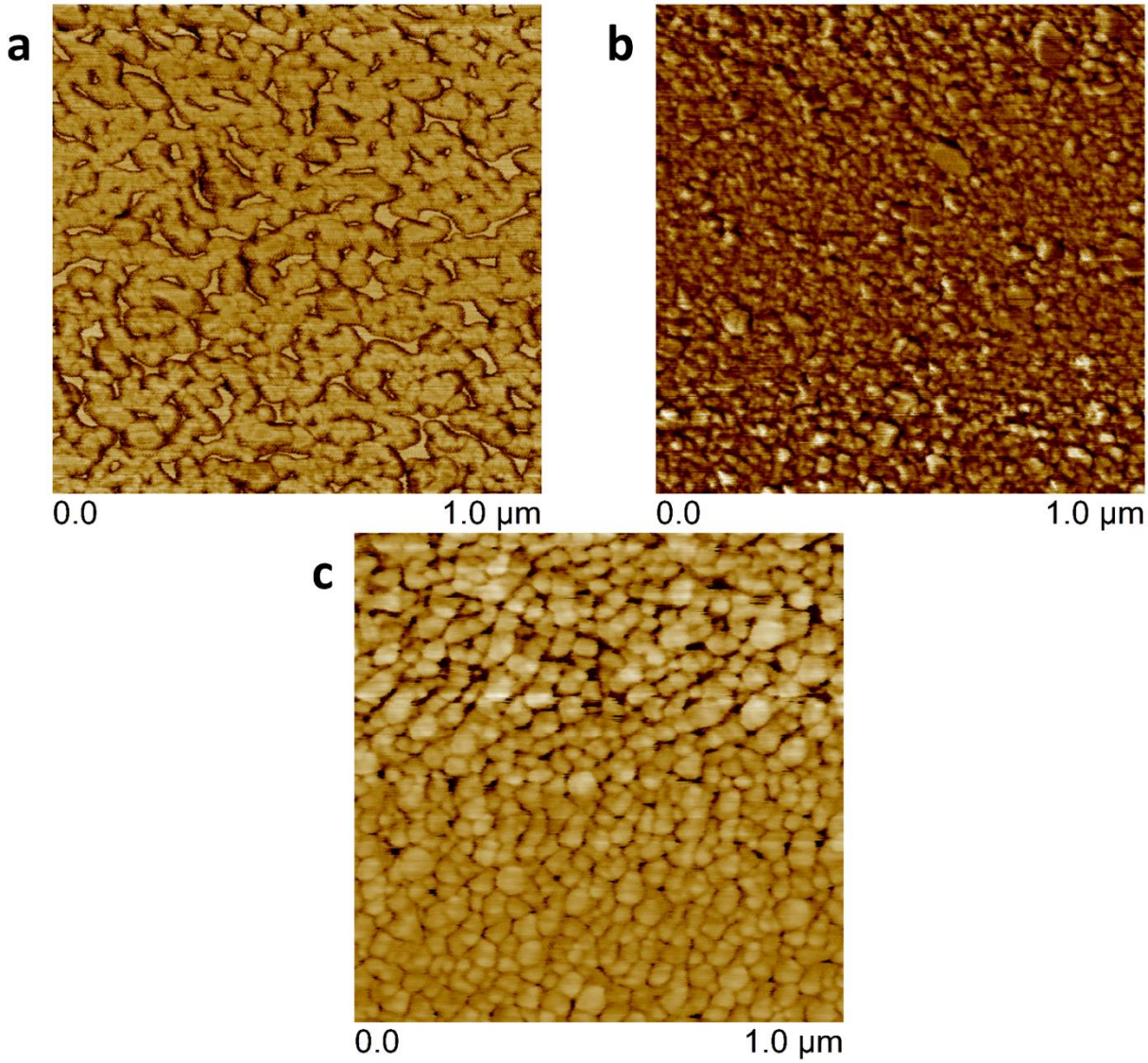

Fig. S3. Atomic force microscope phase images of (a) Ag 8nm, (b) TiO_2 30nm-Ag 8nm, (c) TAI electrode.

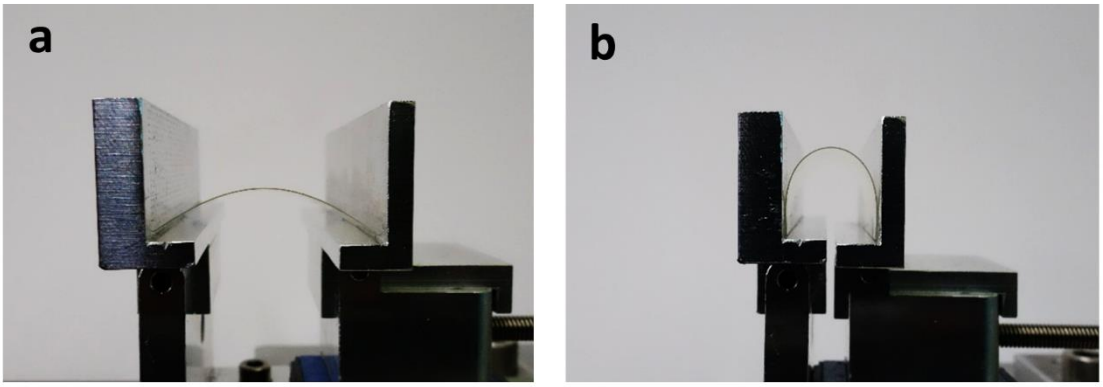

Fig. S4. Mechanical jig holding sample (1 x 1 inch) with radius of curvature (a) 10mm, (b) 3mm.

Table S1. Figure-of-merit (FoM) σ_{DC}/σ_{OP} values of different TC based on OMD structure.

Reference	**Structure**	**FoM**
This work	TiO_2/Ag/ITO	497.8
ITO (commercial)	ITO (135nm)	250
Ref. 7	ZnO/SAM*/Ag/SAM/ZnO	259
Ref. 8	ZTO/Ag/ZTO	410
Ref. 9	MoO_3//Ag/MoO_3	195
Ref. 16	MoO_3/Au/Ag/MoO_3	96
Ref. 21	Al-Ag/ZnO	181
Ref. 22	ZnO/AgO_x/ZnO	180

*SAM: Self assembled monolayer

Supporting Information

Click here to download Supporting Information: SI.docx

Click here to download Production Data: Figure 1.tif

Click here to download Production Data: Figure 2.tif

Click here to download Production Data: Figure 3.tif

Click here to download Production Data: Figure 4.tif

Click here to download Production Data: Figure 5.tif

Click here to download Production Data: Figure 6.tif

Click here to download Production Data: Figure for the Table of Contents.docx